Scalable Modeling of Carbon Tetrachloride Migration in the Deep Vadose Zone at the Hanford Site Using the STOMP Simulator

M. D. White*, M. Oostrom, M. L. Rockhold, and M. Rosing

ABSTRACT

Numerical simulation has been applied in support of the U.S. Department of Energy's (DOE's) efforts to characterize the nature and distribution of carbon tetrachloride contamination in the deep vadose zone at the Hanford site, near Richland, Washington. Three-dimensional simulations were executed using layered and heterogeneous distributions of soil properties to investigate the vertical and lateral distribution of carbon tetrachloride beneath its release point (216-Z-9 trench) and the effects of soil vapor extraction. The complexity of the modeled physical processes, namely, the nonlinearities associated with multifluid subsurface flow, including phase transitions and hysteresis in the relative permeability-saturation-capillary pressure functions, limits the grid resolution when executed using single processor computers. To achieve higher grid resolutions and acceptable detail in the simulation results for subsurface distribution and remediation of carbon tetrachloride, execution on multiple processors was required. This paper describes and demonstrates a scalable implementation of a multifluid subsurface flow and transport simulator, STOMP, with capabilities for volatile organic compounds. Developing scientific software for execution on parallel computers has unique challenges. The guiding objectives for developing this scalable code were to keep the source coding readable and modifiable by subsurface scientists, to allow for both sequential and scalable processing, and to depend on domain scientists for code parallelization and scalable linear system solvers.

M. D. White, Hydrology Group, Pacific Northwest National Laboratory, P. O. Box 999, MSIN K9-33, Richland, WA 99352; M. Oostrom, Hydrology Group, Pacific Northwest National Laboratory, P. O. Box 999, MSIN K9-33, Richland, WA 99352; M.

L. Rockhold, Hydrology Group, Pacific Northwest National Laboratory, P. O. Box 999, MSIN K9-33, Richland, WA 99352; M. Rosing, Peak Five, Fort Collins, CO.
*Corresponding author (mark.white@pnl.gov).

Submitted 1 April 2007.
Revised manuscript submitted on August 27.

INTRODUCTION

Subsurface pollution of soil and groundwater by nonaqueous phase liquids (NAPLs) poses a persistent environmental problem as it contaminates freshwater resources for drinking and irrigation. From a subsurface flow and transport perspective, NAPLs are classified as being either lighter or denser than water, volatile or nonvolatile under ambient conditions, and spreading or nonspreading. The migration behavior of NAPLs through the subsurface, in particular through the vadose zone, depends on their density, viscosity, volatility, and spreading coefficient characteristics and on the transport and soil-moisture characteristics of the porous geologic media through which it travels. Much of the difficulty in remediating subsurface environments contaminated with NAPLs is associated with identifying the nature and distribution of the contaminant. Remediation of dense nonaqueous phase liquid (DNAPL) that has entered the subsurface via disposals, spills, and leaks is considered the most challenging class of problems facing the environmental science community (Johnson et al., 2004). The carbon tetrachloride contamination of the subsurface beneath the 216-Z-9 trench at the Hanford Site, near Richland, Washington typifies the above mentioned general characteristics of NAPL transport behavior and contaminants.

Numerical simulation capabilities for predicting the complex migration behavior (including residual NAPL formation in the vadose zone) of volatile dense organics, such as carbon tetrachloride, have become available to the scientific community (Falta et al., 1992; Oostrom et al. 2005; Piepho, 1996; White et al., 2004). Whereas these computational capabilities have allowed subsurface scientists to investigate laboratory- and field-scale problems, the complexity of the numerical solution limits the computational domain size and thus grid resolution for a particular physical domain. As a general rule, for nonlinear multifluid subsurface flow and transport simulators, execution on a single processor computer is limited to less than $1x10^5$ unknowns. If thermal gradients are ignored (i.e., isothermal conditions are assumed), resolving carbon tetrachloride subsurface flow and transport problem requires the solution of three coupled nonlinear equations at each grid cell, thus reducing the practical number of grid cells to $3x10^4$. For many investigations this

provides sufficient grid resolution; the metric being independency of simulation results with increased grid resolution.

For investigations that require more grid resolution than that afforded by sequential implementations of multifluid subsurface flow and transport simulators, one solution is to increase the number of processors. Assuming perfect linear scaling (i.e., no execution penalties for additional processors), executing on 64 processors would allow the use of $2x10^6$ grid cells on an isothermal carbon tetrachloride subsurface flow and transport problem. At a more realistic ½ scaling factor, the grid resolution is reduced to $1x10^6$ grid cells. Whereas this approach is limited by the number of processors available on a computer (e.g., 256), it does provide subsurface scientists with analytical tools for solving previously intractable problems. This paper describes the conversion and application of a sequential simulator (STOMP-WOA) to scalable form using a preprocessor, controlled through directives embedded in the sequential code. The principal objective of the developed parallelization approach was to keep the source coding readable and modifiable by subsurface scientists and engineers (leaving the bulk of the parallelization to the preprocessor), to allow both sequential and parallel execution of the simulator, and to provide access to a variety of scalable linear system solvers and preconditioners.

BACKGROUND

Plutonium recovery activities at the Plutonium Finishing Plant (PFP) complex on the Hanford Site, near Richland, Washington, resulted in the disposal of organic and aqueous waste via cribs, tile fields and French drains. Approximately, 13.4 million liters of liquid waste were disposed in the 216-Z-9 trench, 216-Z-1A tile field and 216-Z-18 crib. This waste contained 363 to 580 m^3 of liquid carbon tetrachloride (CCl_4) combined with lard oil, tributyl phosphate (TBP) and dibutyl butyl phosphonate (DBBP). By the mid-1980s, dissolved CCl_4 was found in the unconfined aquifer beneath the PFP complex, and in late 1990 the U.S. Environmental Protection Agency (EPA) and the Washington State Department of Ecology requested an expedited response to minimize additional CCl_4 contamination of the groundwater. In an effort to cleanup the CCl_4 contamination at the site, two remediation technologies were applied; soil vapor extraction (SVE) in the vadose zone, and pump and treat

(P&T) in the saturated zone. Between 1991 and 2006, about 79,000 kg CCl_4 was removed at the Hanford site using a multiple-well SVE system, of which 54,300 kg from the subsurface of the 216-Z-9. Between 1994 and 2006, the P&T system produced 10,200 kg of CCl_4 from the unconfined aquifer.

Inexact estimates of the disposed CCl_4 inventory surrounding the PFP complex, conducted by Last and Rohay (1993) suggested that 21% was lost to the atmosphere, 12% was contained in the vadose zone, as aqueous-dissolved, solid-sorbed, or gaseous-vapor, and 2% resided in the saturated zone, as aqueous-dissolved CCl_4. The remaining 65% was unaccounted, perhaps present as residual or mobile NAPL in the vadose and saturated zones. Numerical modeling of CCl_4 migration and remediation in the subsurface beneath the 216-Z-9 has been limited to a two-dimensional Cartesian conceptual model of the site (Piepho, 1996) and a two-dimensional cylindrical model surrounding a passive vapor extraction well (Ellerd et al., 1999), and layered three-dimensional domains (Oostrom et al., 2004; 2006; 2007).

Piepho's simulations were conducted with MAGNAS (Huyakorn et al., 1994), a three-dimensional, finite-element, numerical model that simulates the flow of water, NAPL, and gas, and considered scenarios involving stagnant and flowing groundwater and DNAPL residual saturations of 10^{-4} and 10^{-2}. The simulations additionally included an active soil vapor extraction well at the edge of the domain. Simulation results indicated that between 66% and 90% of disposed CCl_4 inventory remained in the vadose zone, depending on the assigned residual DNAPL saturation. Soil vapor extraction from the single well was reported to have removed less than 0.5% of the total disposed CCl_4 inventory over a six-year operation period. Ellerd et al.'s simulations of a passive vapor extraction system were conducted with a groundwater flow code, using the approximations developed by Massmann (1989). Calibration of the gas flow model was conducted against an observation well screened from 58 to 61.5 m (66-m groundwater depth), by adjusting the gas permeability and saturation of the formation layers. Once calibrated, simulations of a passive vapor extraction well operating on barometric pressure variations agreed with field recoveries (i.e., approximately 15 kg of CCl_4 from the PFP complex site per

year). Ground surface seals surrounding the extraction well were shown to enhance gas flow and CCl_4 recovery.

Oostrom et al. (2004; 2006; 2007) conducted three-dimensional modeling to enhance the current conceptual model of CCl_4 distribution beneath the major disposal site (216-Z-9). The simulations, using the Water-Oil-Air (WOA) mode of the STOMP simulator (White and Oostrom, 2007), focused on migration of dense, nonaqueous phase liquid (DNAPL) consisting of CCl_4 and co-disposed organics under scenarios with differing sediment properties, sediment distribution, waste properties, and waste disposal history. Simulation results support a conceptual model for CCl_4 distribution where CCl_4 in the DNAPL phase migrated primarily in a vertical direction below the disposal site and where some DNAPL likely migrated across the water table into the regional aquifer. Results from Oostrom et al. (2004; 2005; 2007) also show that the lower permeability Cold Creek Unit retained more DNAPL within the vadose zone than other hydrologic units during the infiltration and redistribution process. Due to the relatively high vapor pressure of the CCl_4, the simulated vapor plumes were extensive and influenced by density-driven advection. Any continued migration of CCl_4 from the vadose zone to the groundwater is likely through interaction of vapor phase CCl_4 with the groundwater and not through continued DNAPL migration. Additional simulations assessed the impacts of soil vapor extraction (SVE) as a remediation method. These simulations showed rapid CCl_4 removal associated with the assumed local equilibrium of CCl_4 between the phases. Additional effort is needed to enhance the understanding of rate-limited volatilization to improve simulation of the SVE process and to provide a basis for refining the design and operation of SVE systems.

MATHEMATICAL MODEL

All simulations were executed assuming isothermal conditions, no chemical reactions, and a NAPL with fluid properties representative of the DNAPL disposed at the 216-Z-9 (Oostrom et al., 2004). The DNAPL properties of the mixture are listed in Table 1. Since CCl_4 is the major component of the disposed DNAPL and this mode of the simulator only supports a single-component DNAPL, CCl_4 has been chosen as the name for the DNAPL. With these assumptions the flow and transport of CCl_4

through the subsurface can be described by three component mass conservation equations (i.e., water, air, CCl_4), over four phases (i.e., aqueous, NAPL, gas, and solid). Equilibrium partitioning is assumed of the components over the phases. Expressed in partial differential form, the mass conservation equations can be written as

$$\frac{\partial}{\partial t}\left[\sum_{\gamma=s,l,n,g}\left(n_D\,\omega_\gamma^i\,\rho_\gamma\,s_\gamma\right)\right] = -\sum_{\gamma=l,n,g}\left(\nabla\,\mathbf{F}_\gamma^i + \nabla\,\mathbf{J}_\gamma^i\right) + m^i,\ \textit{for } i = w, o, a \qquad [1]$$

where n_D is the diffusive porosity, ω_γ^i is the mass fraction of component i in phase □, ρ_γ is the density (kg/m^3) of phase □, s_γ is the saturation of phase □□□ $\mathbf{F}_\gamma^i$ □is the advective flux vector (kg/m^2 s) of component i in phase □, $\mathbf{J}_\gamma^i$ is the diffusive flux vector (kg/m^2 s) of component i in phase □, and m^i is the mass source rate (kg/m^3 s) of component i. The advective flux vector is a function of pressure gradient, gravitational buoyancy, phase relative permeability, and phase viscosity as

$$\nabla\,\mathbf{F}_\gamma^i = -\frac{\omega_\gamma^i\,\rho_\gamma\,k_{r\gamma}\,\mathbf{k}}{\mu_\gamma}\left(\nabla\,P_\gamma + \rho_\gamma\,g\,\mathbf{z}_g\right) \qquad [2]$$

where $k_{r\gamma}$ is the relative permeability of phase γ, $\mathbf{k}$ is the intrinsic permeability tensor (m^2), μ_γ is the viscosity (Pa s) of phase γ, P_γ is the pressure (Pa) of phase γ, g is the acceleration of gravity (m/s^2), and $\mathbf{z}_g$ is the gravitational unit vector. The diffusive flux vector is a function of the molar density gradient, phase saturation, tortuosity, and diffusion coefficient as

$$\nabla\,\mathbf{J}_\gamma^i = -\tau_\gamma\,n_D\,s_\gamma\,D_\gamma^i\,\nabla\left(\frac{M^i}{M_\gamma}\,\rho_\gamma\,\chi_\gamma^i\right) \qquad [3]$$

where τ_γ is the tortuosity factor of phase γ, D_γ^i is the molecular diffusion coefficient (m^2/s) of component i in phase γ, M^i is the molecular weight (kg/kmol) of component i, M_γ is the molecular weight (kg/kmol) of phase γ, and χ_γ^i is the mole fraction of component i in phase γ.

The aqueous phase comprised primarily liquid water with dissolved air and CCl_4; the NAPL comprised liquid CCl_4 only; the gas phase comprised noncondensible air, water vapor and CCl_4 vapor; and the solid matrix comprised porous media matrix and sorbed CCl_4. The constitutive equations that relate the primary unknowns of the governing equations to secondary unknowns, which include the phase thermodynamic and transport properties, phase saturation, and phase relative permeability, are nonlinear. Solutions for the combined governing and constitutive equations were obtained at discrete grid locations and points in time, using finite-difference based spatial discretization and Euler backward temporal discretization. Nonlinearities were resolved using multivariate Newton-Raphson iteration. Primary variable switching is used to handle phase transitions, appearances, and disappearances. A more complete description of the constitutive equations and numerical solution schemes is provided in the theory guide for the STOMP[1] simulator (White and Oostrom, 2000; White and Oostrom, 2006). A critical component of the constitutive equations for the Hanford Site application of CCl_4 migration is the calculation of residual NAPL in the vadose zone. The details of the theory and its implementation into the STOMP simulator are provided by White et al. (2004).

SCALABLE IMPLEMENTATION

The STOMP simulator is a collection of operational modes, implementations, and modules for solving multifluid subsurface flow and reactive transport problems. Operational modes are distinguished by the solved coupled flow and transport equations. The subject operational mode solves the conservation equations for water, air, and oil mass and is known as STOMP-WOA. Implementations are either sequential or scalable. Sequential implementations of the simulator were written in FORTRAN 77, with an option for dynamic memory allocation if compiled with a Fortran 90 compiler. Although some Fortran compilers offer auto-parallelization, the scalable implementation is generally executed on a single processor computer. Scalable implementations were written in Fortran 90, but currently do not take advantage of the dynamic memory capabilities of the language. Modules are

[1] http://stomp.pnl.gov

additional capabilities above the standard flow and transport schemes, such as, reactive transport (White and McGrail, 2005) , multifluid well models, and sparsely vegetated surface models (Ward et al., 2005).

The sequential implementations of the STOMP simulator were written first and represent the standard form of the simulator. Not all sequential operational modes of the simulator have been converted to scalable form. Conversions have occurred based on the need for parallel computing. In developing the scalable implementations of the STOMP simulator, the choice was made to rewrite the simulator to take advantage of the parallel-programming structures built into the Fortran 90 language. The guiding objectives for developing the parallel implementation of the simulator were to 1) keep the source coding readable and modifiable by subsurface scientists, 2) allow both sequential and parallel execution, 3) leave the bulk of the parallelization to computer scientists, and 4) consign the parallel linear system solvers to applied mathematicians. The resulting coding scheme was to embed directives into the Fortran 90 coding that defined the parallelism. These directives appear as Fortran 90 comments, which means that the code can be compiled and executed as a conventional (i.e., sequential implementation). This compilation option also allows for conventional debugging during the development stage. To realize the scalable implementation of the simulator, the embedded directives in the code are interpreted by a Fortran Preprocessor (FP) (Rosing and Yabusaki, 1999). The FP comprises three components: 1) the preprocessor program, 2) the directive language (DL), and 3) the library. The FP is actually a generic preprocessor that has been programmed with a library of directives, written in a C-like language, called DL (Rosing, 2000) to operate on and manipulate Fortran 90 code fragments. Output from executing the FP program on the STOMP source code is new source coding with redimensioned arrays whose memory is distributed over the processors (i.e., compute nodes), calls to the MPI library (Gropp et al., 1999), and calls to the FP library.

Computational Domain Discretization

The STOMP simulator uses integral volume finite differencing for spatial discretization and backward Euler differencing for temporal discretization of the

governing partial differential flow and transport equations. For spatial discretization it is further assumed that the grid system is orthogonal and structured; where, a structured grid implies that a non-boundary grid cell has two, four, and six neighbors, in one-, two-, and three-dimensional domains, respectively. Field variables (e.g., temperature, phase pressure, phase saturation, phase relative permeability, mole fraction) are define at the grid centroids. Flux variables (e.g., component mass flux, energy flux) are defined at the centroid of the interfacial surface between two grid cells or the centroid of a boundary surface. Both field and flux variables are multi-dimensional arrays, with the first three indices being used to define the grid-cell coordinates. The FP has been programmed with the assumption that the computational domain is discretized into a regular grid of processors (i.e., a contiguous subdomain of the structured grid is assigned to a processor). Grid cells that are within the assigned section of a processors subdomain are defined to be local to the processor. A three-dimensional computational domain, representing a three-dimensional physical domain, can be discretized into a three-, two-, or one-dimensional grid of processors. In general, the processor domain dimensionality must be less than or equal to the computational domain dimensionality.

Field and flux variables are distributed over the processor domain according to user specifications, which include: 1) dimensions to distribute, 2) number of ghost cells, and 3) number of boundary cells. For a three dimensional computational domain, the user may specify that all three dimensions are distributed, that any two dimensions are distributed, or that any one dimension is distributed over the processors. Ghost cells refer to the number of computational grid cells that are duplicated in each of the distributed directions. Without ghost cells, fluxes on grid cell surfaces that coincide with process boundaries would require field variables from two different processors. Ghost cells, therefore, allow flux calculations to remain local to the processors. Updating of the ghost cells is handled automatically by the FP. As flux variables are defined on computational domain grid surfaces, there is the potential for having misaligned distributions of flux and field variables over the processor distributions. The FP allows the user to define upper and lower boundary cells, which allows the flux variables to be aligned with field variables; thereby, keeping all flux calculations local to the processor.

The default boundary condition in the STOMP simulator is a zero-flux boundary. Boundary conditions occur on the computational domain boundary surfaces and on the boundary surfaces between active and inactive nodes. User-assigned boundary conditions specify conditions on a boundary surface associated with a single grid cell, and are generally local calculations (i.e., involving a single processor). The FP allows for this type of calculation by delineating sections of code as being serial. To delineate a section of code as being serial, bounding directives are embedded in the Fortran code. Within serial sections of code, the FP provides additional support, through "shared variable" directives for nondistributed variables or arrays that need to be consistent on all processors. Writes to a shared variable, within a serial section of code, are broadcast to all processors. For example, a shared variable could be used in conjunction with linked boundary surfaces; where, one boundary condition is dependent on an adjacent boundary condition (e.g., hydraulic gradient type boundary conditions).

In addition to handling distributed arrays, parallelization of loops over grid cells and serial code sections, the FP automatically translates input and output statements. The general approach used by the FP is to execute all input and output on processor zero (i.e., the base processor of a processor cluster). The translation of the Fortran read and write statements depends on whether the variable being input or output is distributed. For non-distributed variables, Fortran read and write statements are executed from processor zero, and the data are then broadcast to all processors; therefore, replicating the data on all processors. For distributed variables, the semantics depend on whether the data are formatted or unformatted. For formatted data, Fortran read and write statements are executed from processor zero, followed by a global broadcast. For unformatted data, special FP and MPI library calls are executed for the data distribution operations. One limitation of the FP is that it is not possible to mix distributed and non-distributed variables in an unformatted Fortran read or write statement.

HYDROGEOLOGIC MODELS

The hydrogeologic models for the subject simulations comprise a distribution of soil types (i.e., geologic model) and hydrologic properties for each defined soil type. Two types of hydrogeologic models were employed during this investigation; a layered model and a heterogeneous model. In the layered model, 12 soil types were distinguished and the distribution of soils were defined through a geologic interpretation of 21 boreholes within the immediate vicinity of the 216-Z-9 trench. Hydrologic properties for each of the 12 soil types were assigned by mapping these soil types to various soil/sediment classes for which data were available (Khaleel et al., 2001; Khaleel and Freeman, 1995) for the Hanford Site. In the heterogeneous model, every grid cell was assigned unique hydrologic properties. Compared with the layered geologic domain, which uses homogeneous hydrologic parameters within each stratigraphic layer/region of the domain, the heterogeneous geologic domain has different hydrologic parameters for each grid cell, while honoring the average hydrologic parameters of the stratigraphic layers. Parameterization of the hydrologic properties for the heterogeneous model was realized using either a pedotransfer function (PTF) or similar media scaling (SMS) method.

Layered Geologic Model

The geologic model surrounding the 216-Z-9 trench for the subject simulations was developed in three stages, each covering successively smaller nested domains. The outer-most geologic model, a regional-scale domain, was developed to link groundwater modeling to the smaller domains through boundary conditions. The intermediate geologic model, a local-scale domain, was developed to define the groundwater elevations and gradients of the principal CCl_4 disposal facilities (i.e., Z-9, Z-1A, and Z-18). The inner-most geologic model, a site-scale domain (i.e., beneath the 216-Z-9 trench), was developed as the computational domain for the subject simulations. The boundaries of the regional-scale domain were set to include primary recharge or discharge areas, thereby acting as logical hydrologic boundaries. The boundaries include important liquid disposal areas: the 216-U-14 ditch to the east, the 216-U-pond to the south, the 200-ZP-1 injection wells to the west, and the old 216-T-4 pond to the north. Geologic data for the regional-scale domain was derived from 172 groundwater wells. Geologic data for the local-scale

domain was derived from 215 boreholes (i.e., groundwater wells, dry wells, and soil borings). For the site-specific domain, geologic data from 21 boreholes within the immediate vicinity of the 216-Z-9 trench was included. The collected geologic data were mapped to a single set of stratigraphic units, the new Standardized Stratigraphic Nomenclature (DOE, 2002). Discrepancies between geologic data sets and anomalous areas in the resulting geologic models created by EarthVision were resolved using driller's, geologist's and geophysical logs, and particle-size, calcium-carbonate, and moisture-content data, along with data from the Hanford Well Information System. A three-dimensional view of the resulting geologic model with a cut-out beneath the 216-Z-9 disposal site is shown in Figure 1.

Heterogeneous Geological Model

Alluvial sediments at the Hanford Site were deposited in a series of very high energy cataclysmic flooding events, yielding a heterogeneous geology with a hierarchy of scales, ranging from mm-scale laminations and cross-bedding, to cm-scale silt lenses, to much thicker sand layers. A fundamental problem in numerically simulating multifluid flow and transport processes for these heterogeneous deposits is the disparity among the scales of actual physical heterogeneities, characterization or measurement, and computational grid cells. The layered-geologic model ignores the heterogeneities within the specified stratigraphic units. To address these heterogeneities, geostatistical stochastic conditional simulation (Deutsch and Journel, 1998) was used to parameterize hydrologic properties for each grid cell within the computational domain. This approach uses geostatistical methods for which parameters are conditioned to hard data (i.e., determined from measurements on core samples) or soft data (i.e., field-measured water contents from geophysical well logging or core samples, or grain-size distributions) (Rockhold, 1999; Rockhold et al. 1993). The resulting heterogeneous geologies are realizations of equally drawn random fields of spatially-correlated parameter or property distributions that preserve the data at their actual measurement locations, as well as the histogram and spatial auto-correlation and cross-correlation data structure. The following two sections provide brief descriptions of the basic steps used for parameterization of heterogeneous models using the PTF and SMS methods.

Pedotransfer Function Method

The pedotransfer function (PTF) method involved a series of steps: 1) computing metrics (i.e., inclusive graphic standard deviation, σ_{IG} and d_{50} grain-size diameter) from grain-size data, 2) developing a pedotransfer function to estimate hydraulic parameters from the grain-size distribution metrics, 3) determining spatial correlation lengths using a variogram analysis of the grain-size distribution metrics, 4) stochastically simulating the grain-size metrics on a fine-scaled domain, 5) generating hydraulic parameters at each fine-scale grid cell using the pedotransfer functions, and 6) upscaling the hydraulic parameters to a coarser computational grid for the numerical simulation of multifluid flow and transport processes. Grain-size distribution data for the Hanford Site (i.e., more than 40,000 sediment samples) and for the immediate vicinity of the 216-Z-9 trench (i.e., 523 samples) were used to generate metrics by fitting a continuous function to these data. Pedotransfer functions were then generated between the grain-size-distribution metrics and hydraulic parameters (i.e., intrinsic permeability, porosity, soil-moisture retention characteristics). Directional variogram analyses were then performed on normal score transforms (Deutsch and Journel, 1998) of the σ_{IG} and the d_{50} data sets for six hydrostratigraphic units. The hydrologic properties for the basal basalt unit and an intermediate caliche layer (i.e., a consolidated and cemented but relatively brittle sedimentary deposit) were assigned deterministic parameters, because these units are either hard rock or consolidated and relatively brittle, making grain-size data not useful for estimating hydraulic properties.

The variogram parameters for σ_{IG} and d_{50} for each of the six hydrostratigraphic units were used as inputs to the SGSIM program (Deutsch and Journel, 1998), yielding multiple, equally drawn realizations of the metrics σ_{IG} and d_{50} on the fine-scale grid. The fine-scale grid consisted of 3,022,272 grid cells, with uniform 5-m spacing horizontally and uniform 0.5-m spacing vertically. The realizations are considered conditional in that they honor the grain-size distribution metrics spatially, while also preserving the histogram and auto-correlation structure of the variables (Deutsch and Journel, 1998). The metrics, σ_{IG} and the d_{50}, were found to be

uncorrelated, eliminating the need to account for cross-correlation. With the σ_{IG} and d_{50} metrics computed for each grid cell, hydraulic parameters were derived using pedotransfer functions (Oostrom et al., 2006). The computational grid comprised 1,075,250 grid cells, where spacing varied from 0.91 to 20 m horizontally and from 0.5 to 3 m vertically.

Procedures for scaling parameters between the fine-scale and computational grid were relatively straightforward. Diffusive porosity was upscaled using volume averaging, as

$$\left(n_D\right)^C = \frac{\sum_{j=1}^{n} \left(n_D\right)_j^F \left(V\right)_j^F}{\sum_{j=1}^{n} \left(V\right)_j^F} \quad [5]$$

where $\left(V\right)_j^F$ is the volume of the partial or complete fine-scale grid cell j, $\left(n_D\right)_j^F$ is the diffusive porosity of the fine-scale grid cell j, n is the number of fine-scale grid cells that are partially or completely within the computational grid cell, and $\left(n_D\right)^C$ is the diffusive porosity for the computational grid. Retention characteristic parameters that define the relationships between relative permeability, capillary pressure, and saturation (k-s-P relations) were also upscaled using volume averaging, according to Equation [5]. Lower bounds for the intrinsic permeability for each principal direction were computed from area-weighted arithmetic mean of the length-weighted harmonic mean of the fine-scale intrinsic permeability, as

$$\left(k_x\right)_L^C = \sum_{k=1}^{nz} \left[\sum_{j=1}^{ny} \left\{ \left(dy_j\, dz_k\right) \left[\sum_{i=1}^{nx} dx_i \Big/ \sum_{i=1}^{nx} \frac{dx_i}{\left(k_x\right)_i^F} \right] \right\} \Big/ \sum_{j=1}^{ny} \left(dy_j\, dz_k\right) \right] \quad [6a]$$

$$\left(k_y\right)_L^C = \sum_{k=1}^{nz} \left[\sum_{i=1}^{nx} \left\{ \left(dx_i\, dz_k\right) \left[\sum_{j=1}^{ny} dy_j \Big/ \sum_{j=1}^{ny} \frac{dy_j}{\left(k_y\right)_j^F} \right] \right\} \Big/ \sum_{i=1}^{nx} \left(dx_i\, dz_k\right) \right] \quad [6b]$$

$$\left(k_z\right)_L^C = \sum_{i=1}^{nx}\left[\sum_{j=1}^{ny}\left\{\left(dx_i\,dy_j\right)\left[\sum_{k=1}^{nz} dz_k \Big/ \sum_{k=1}^{nz}\frac{dz_k}{\left(k_z\right)_k^F}\right]\right\}\Big/\sum_{j=1}^{ny}\left(dx_i\,dy_j\right)\right] \quad [6c]$$

where $\left(k_x\right)_L^C, \left(k_y\right)_L^C, \left(k_z\right)_L^C$ are the lower-bound intrinsic permeability (m^2) on the computational grid in the principal directions, nx, ny, nz are the number of fine-scale grid cells in the principal directions, dx, dy, dz are the dimensions (m) of the fine-scale grid cells in the principal directions, and $\left(k_x\right)_i^F, \left(k_y\right)_j^F, \left(k_z\right)_k^F$ are the intrinsic permeability (m^2) on the fine-scale grid in the principal directions. Upper bounds for the intrinsic permeability for each principal direction were computed from the length-weighted harmonic mean of the area-weighted arithmetic mean of the fine-scale intrinsic permeability, as

$$\left(k_x\right)_U^C = \sum_{i=1}^{nx} dx_i \Big/ \sum_{i=1}^{nx}\left[dx_i \Big/ \sum_{k=1}^{nz}\left\{\sum_{j=1}^{ny}\left[dy_j\,dz_k\left(k_x\right)_i^F\right]\Big/\sum_{j=1}^{ny}\left(dy_j\,dz_k\right)\right\}\right] \quad [7a]$$

$$\left(k_y\right)_U^C = \sum_{j=1}^{ny} dy_j \Big/ \sum_{j=1}^{ny}\left[dy_j \Big/ \sum_{k=1}^{nz}\left\{\sum_{i=1}^{nx}\left[dx_i\,dz_k\left(k_y\right)_j^F\right]\Big/\sum_{i=1}^{nx}\left(dx_i\,dz_k\right)\right\}\right] \quad [7b]$$

$$\left(k_z\right)_U^C = \sum_{k=1}^{nz} dz_k \Big/ \sum_{k=1}^{nz}\left[dz_k \Big/ \sum_{j=1}^{ny}\left\{\sum_{i=1}^{nx}\left[dx_i\,dy_j\left(k_z\right)_k^F\right]\Big/\sum_{i=1}^{nx}\left(dx_i\,dy_j\right)\right\}\right] \quad [7c]$$

where $\left(k_x\right)_U^C, \left(k_y\right)_U^C, \left(k_z\right)_U^C$ are the upper-bound intrinsic permeability (m^2) on the computational grid in the principal directions. The upper and lower bounds for intrinsic permeability are referred to as the Cardwell and Parsons bounds (Cardwell and Parsons, 1945; Renard and de Marsily, 1997). Effective intrinsic permeability values for each computational grid cell were computed as (Malik and Lake, 1997; Li et al. 2001), as

$$\left(k_x\right)^C = \sqrt{\left(k_x\right)_L^C\left(k_x\right)_U^C} \quad [8a]$$

$$\left(k_y\right)^C = \sqrt{\left(k_y\right)_L^C\left(k_y\right)_U^C} \quad [8b]$$

$$\left(k_z\right)^C = \sqrt{\left(k_z\right)_L^C\left(k_z\right)_U^C} \quad [8c]$$

where $(k_x)^C$, $(k_y)^C$, $(k_z)^C$ are the effective intrinsic permeability (m^2) on the computational grid in the principal directions. Color-scaled images of the vertical intrinsic permeability and Brooks-Corey (Brooks and Corey, 1964) entry pressure head distributions for the computational grid using the pedotransfer function approach are shown in Figures 2a and 2b.

Similar Media Scaling Method

The similar media scaling (SMS) method (Miller and Miller, 1956) involved a series of steps: 1) computing d_{50} grain-size diameter from grain-size data, 2) determining spatial correlation lengths using a variogram analysis of the d_{50} grain-size diameter, 3) stochastically simulating the d_{50} grain-size diameter on a fine-scaled domain, 4) generating hydraulic parameters at each fine-scale grid cell using the similar media scaling method, and 5) upscaling the hydraulic parameters to a coarser computational grid for the numerical simulation of multifluid flow and transport processes. The similar media scaling method is founded on the notion that for geometrically similar porous media, hydrologic properties are related through known functions of characteristic lengths. For this investigation the d_{50} grain-size diameter was used as the characteristic length. Values for the saturated hydraulic conductivity (or intrinsic permeability) and Brooks-Corey air-entry pressure were computed from the spatial realizations of d_{50} grain-size diameter distributions on the fine-scale grid using the following equations, respectively

$$K_s = K_s^* \left(\frac{d_{50}}{d_{50}^*} \right)^2, \; or \; k = k^* \left(\frac{d_{50}}{d_{50}^*} \right)^2 \qquad [9]$$

$$h_d = h_d^* \left(\frac{d_{50}^*}{d_{50}} \right) \qquad [10]$$

where K_s is the saturated hydraulic conductivity (m/s), K_s^* is the saturated hydraulic conductivity of the stratigraphic unit in the layered model, d_{50} is the conditionally simulated value of the median grain diameter generated using the SGSIM program,

d_{50}^{*} is the median grain diameter of the stratigraphic unit, k is the intrinsic permeability (m^2), k^{*} is the intrinsic permeability (m^2) of the stratigraphic unit, h_d is the Brooks-Corey air-entry pressure head (m), and h_d^{*} is the Brooks-Corey entry pressure head (m) of the stratigraphic unit. The remaining hydrologic parameters (i.e., porosity, residual saturation, Brooks-Corey lambda) were assigned those values used in the layered geology. The similar media scaling parameterization implicitly assumes that porous media within a stratigraphic unit are geometrically similar. As for the pedotransfer function parameterization, the hydrologic parameters for the basal basalt unit and an intermediate caliche layer were assigned deterministic parameters. Color-scaled images of the vertical intrinsic permeability and Brooks-Corey (Brooks and Corey, 1964) entry pressure head distributions for the computational grid using the similar media scaling approach are shown in Figures 3a and 3b.

NUMERICAL SIMULATIONS

Boundary and Initial Conditions

The 216-Z-9 trench site is located in an arid environment above a deep vadose zone, with the regional groundwater flow direction being toward the Columbia River. In developing boundary conditions for the simulations, the atmospheric pressure and precipitation fluctuations were ignored, but the long-term water-table fluctuations and regional gradients were considered. Constant atmospheric gas pressure (Dirichlet-type boundary) and constant flux (i.e., 0.5 cm/yr) of water (Neumann-type boundary) was applied on the top surface of the computational domain. The bottom boundary of the domain was impermeable basalt bedrock and was treated in the numerical simulations as a zero-flux boundary. The vertical boundaries were treated as time-variant hydraulic gradient type boundaries below the water table and as zero-flux boundaries above the water table. The boundary condition variations and cross-domain gradients were derived from observed water levels in wells in the immediate vicinity of the 216-Z-9 trench. The resulting boundary conditions yielded a northing groundwater flow direction. Details of the time-variant boundary conditions can be found in Oostrom et al. (2004). Neumann-type boundary

conditions were imposed for water and DNAPL discharges for the 216-Z-9 trench area during the years that these liquids were disposed (Table 2). DNAPL was allowed to move freely across all boundaries. The initial gas and aqueous phase pressure distributions in the domain at 1954 were obtained by conducting a 10,000-yr simulation using the interpolated 1954 water levels at the south and north boundary and a recharge rate of 0.5 cm/yr. It was further assumed that initially, no DNAPL was present in the domain.

Fluid and Porous Medium Properties

DNAPL fluid properties were measured in the laboratory based on an assumed average fluid composition of 8.8% (v/v) TBP, 14.7% DBBP, 2.9% lard oil, and 73.6% CCl_4 (Last and Rohay, 1993). The obtained values are listed in Table 1. Retention parameters, porosities, and hydraulic conductivities for the units were obtained from Khaleel et al. (2001) and Khaleel and Freeman (1995), and are listed in Table 3. A permeability anisotropy ratio of 10:1 was used. The parameters for the relative permeability-saturation-pressure Van Genuchten (1980) – Mualem (1976) models were converted to equivalent parameters for the Brooks-Corey (1964) - Burdine (1953) models, using the method described by Lenhard et al. (1989). A linear sorption model with a K_d of 0.2 mL/g was applied to all porous media.

Grid Refinement

The computational domain was 440, 540, and 159 m in the west-east, south-north, and top-bottom directions, respectively. The original layered models described by Oostrom et al. (2004; 2006; 2007) were discretized into 27 x 34 x 85 = 78,030 grid blocks. The model was refined near the disposal site and the low permeability Cold Creek Unit. The footprint of the 216-Z-9, with approximate dimensions of 9.1 x 18.3 m, was located near the center at the top of the site-specific domain. The Basalt unit (Figure 1), at an elevation of 42 m, was assumed to form an impermeable bottom boundary. Because the STOMP-WOA (water-oil-air) mode was used, the number of nodes used in these layered simulations translates into 3 x 78,030 = 234,090 unknowns.

To determine the grid for the heterogeneous model simulations, a series of grid refinement simulations was completed. For the layered geological model, simulations were conducted using the previously used 78,030 node (78K) grid and three refined grids for 310,590 nodes (310K), 635,460 nodes (635K), and 1,075,250 nodes (1075K). For the heterogeneous model, grid refinement simulations were conducted using the 78K, 310K, 635K, and 1075K grids for the similar media scaling method only.

Some pertinent statistics of the grid refinement exercises for the layered and heterogeneous model are shown in Table 4 and 5. Table 4 shows that for both models the DNAPL in the computational domain increases with the number of grid blocks, although the increase from the 635K to the 1075K is small. The DNAPL mass that moves across the water table, located approximately 60 m below the ground surface, shows opposite patterns for both models (Table 5). For the layered model, grid refinement reduced lateral spreading due to fluid retention and allowed more DNAPL to move vertically downwards. With increased refinement, the vertical center of mass moved downward, and the second order vertical moment increases. For all practical purposes, the differences between the simulations in terms of phase distributions over time are limited. An example of the differences is shown in Figure 4 for the DNAPL mass. Because the results are relatively close, it can be concluded that the 78K grid block simulations reported by Oostrom et al. (2004; 2005; 2007) were sufficient for the purposes intended.

However, in contrast with the layered systems, the increased volume of DNAPL, for the heterogeneous model, does not translate into a considerable increase in vertical spreading and increased DNAPL movement across the water table. Instead, Table 5 shows that the DNAPL mass that moves across the water table decreases with grid refinement. In addition, the center of mass and the second-order moments remain virtually unchanged. The main reason that the more refined simulations do not show DNAPL mass transfer across the water table, despite the presence of increased DNAPL over the computation domain, is the increase in textural interfaces in the vertical direction. In the vadose zone, these interfaces cause DNAPL to remain at higher saturations in grid blocks with finer materials upstream of coarser materials.

The integrated effect of increased DNAPL storage in upstream finer-grained grid blocks is a decrease in the vertical distance a certain volume is able to travel. Given that the differences between the 635K and 1075K simulations, as shown in Tables 4 and 5, are minimal, and because the 78K and 310K grid block simulations both show DNAPL movement across the water table while the more refined systems do not, it was decided that the 1075K grid block simulations were appropriate for this domain for heterogeneous simulations.

Heterogeneous Model Simulation Results

The primary focus of this paper is the simulations conducted with the heterogeneous geology, using the pedotransfer function (PTF) method and similar media scaling (SMS) method on the high resolution computational domain (i.e., 1075K grid cells) with the scalable implementation of STOMP-WOA. As a reference these simulations were compared against simulations using the layered geology with the 1075K grid. Six simulations using the heterogeneous geology were executed; three realizations for each parameterization method (i.e., PTF and SMS). Heterogeneous model simulations were conducted for three realizations each for both the PTF and the similar media scaling methods. The simulations were conducted with the 1075K grid.

The layered geology simulations (Figure 5a) show nearly constant total CCl_4 mass in the domain, with declining amounts of the CCl_4 being in NAPL form prior to the initiation of the SVE system in 1993. In contrast, the PTF simulations (Figure 5b) show a sharp decrease in total CCl_4 mass after the source period, with nearly all the CCl_4 being gone prior to 1993. The SMS simulations (Figure 5c) differ from the layered geology results in that the total CCl_4 mass declines over time, but not to the extent of the PTF simulations. Since the results of the three realizations for the heterogeneous approaches are quite similar (Figure 6), only the results for Realization 1 were shown for both methods in Figure 5. The PTF-based heterogeneous model results (Figure 5b) show that almost all CCl_4 had been removed from the subsurface by 1993, the year SVE operations started. For this case, no CCl_4 would have been available for removal with the SVE wells.

Figures 7a, b, and c, show phase fluxes at several interfaces for the layered and the two heterogeneous cases. The main differences between the layered and heterogeneous PTF-based simulation is that for the latter case, most CCl_4 has left the domain by gaseous advection, either density- or pressure-driven. The high gas flux is directly related to the permeability field produced by the PTF method. Table 6 shows the median values of the horizontal hydraulic conductivity for the layered and both heterogeneous models. The data show that the values for the PTF-based model are considerably larger than for the other two models. Given similar pressure fields, gas advection is larger in the PTF-based model than in the other model. In addition, density-driven gas advection is more prominent due to the larger hydraulic conductivities. Furthermore, in the heterogeneous models, more CCl_4 is retained due to the increased number of textural interfaces compared to a layered case, allowing the faster moving gas to transport larger amounts of CCl_4 volatilized into the gas phase. We believe that the PTF approach produces unrealistically high hydraulic conductivities leading to excessive volatilization and gaseous transport due to pressure and concentration gradients. The prediction that no CCl_4 is present at 1993 does not correspond to the obtained field recovery of the SVE system.

The simulations with heterogeneous systems based on the similar media scaling method produced CCl_4 distributions (Figure 5c) that are closer to the results produced with the layered model. The most critical difference between the simulation results from the layered geology and SMS parameterization is the DNAPL migration across the water table. With its increased number of textural interfaces, the SMS simulation yields no DNAPL crossing the water table, as the DNAPL is retained in the vadose zone. Dissolved concentrations of CCl_4 have been recorded in the groundwater in the vicinity of the 216-Z-9 trench, but at concentrations below the solubility limit. It is not evident whether DNAPL below the water table provides a source of CCl_4 in the groundwater or if the observed groundwater concentrations result from transport through the gas phase via density-driven advection.

Processor Scaling

All of the simulations with the scalable implementation of STOMP-WOA were executed on the Pacific Northwest National Laboratory's MPP2 computer located in

the Molecular Sciences Computing Facility[2] (MSCF) of the Environmental Molecular Science Laboratory[3] (EMSL). The MPP2 supercomputer has 1960 Itanium-2 processors (Madison, 1.5 GHz) on 980 nodes, configured such that 574 nodes have 10 Gbyte of RAM and 430 Gbyte of local disk space, 366 nodes have 10 Gbyte of RAM and 10 Gbyte of local disk space, 34 nodes are Lustre server nodes, 2 nodes are administrative, and 4 nodes are login. The 980 nodes are connected via a Quadrics QsNetII interconnect, giving the computer 11.8 TFlops peak theoretical performance. For disk space the computer has 9.7 terabytes of combined RAM, 450 terabytes of local scratch disk space, and 53 terabytes on the Lustre shared cluster file system. To investigate the performance of the scalable implementation of the STOMP-WOA simulator for the subject simulations, a series of executions were conducted for the layered model on the 1075K domain using different numbers of processors, from 27 to 256. A plot of execution time versus the number of processors is shown in Figure 8 for both the periods when the DNAPL was imbibing into the subsurface (1955.5 to 1962.5) and when the SVE system was operational (1993-2002). These two periods are recognized as computationally demanding due to the rapid DNAPL infiltration during waste disposal and removal via the gas phase during SVE. For this investigation, the total number of grid cells or unknowns is fixed; therefore, the number of grid cells per processor decreases with increasing number of processors. The scaling performance curve (Figure 8) shows the expected trend of decreasing execution time with increasing processor count, until the inter-processor communications begin to degrade performance.

SUMMARY AND CONCLUSIONS

Numerical simulations were conducted with layered and heterogeneous geologic models to predict the subsurface distribution of CCl_4 that had been discharged in the 216-Z-9 trench at the Hanford Site, near Richland, Washington. Simulations were executed using the scalable versions of the STOMP-WOA simulator (White and Oostrom, 2006), which solves the multifluid flow and transport equations for conservation of water, oil, and air mass, transported through geologic media over

[2] http://mscf.emsl.pnl.gov
[3] http://www.emsl.pnl.gov

the aqueous, NAPL, gas, and solid phases, assuming isothermal conditions. Heterogeneous geologic models of the subsurface environment in the vicinity of the 216-Z-9 trench were developed using the pedotransfer function and similar media scaling methods. Grid refinement sensitivity simulations indicated that 1075K grids were required for the heterogeneous geologic domains. This investigation focused primarily on the simulation of the heterogeneous models, using the scalable implementation of the simulator.

Although the resolution of the 1075K grid does not capture the small-scale heterogeneities observed in the alluvial Hanford sediments, it does introduce texture interfaces between grid cells, which increase the resistance to DNAPL migration. In the vadose zone, DNAPL tends to preferentially accumulate in the finer-grained sediments, which are more abundant in the heterogeneous geologic models. The net effects of the increase in textural interfaces is less vertical migration of the DNAPL, but increased volatilization of the CCl_4 and subsequent migration in the gas phase. Simulation results with the heterogeneous geologic models showed significantly higher amounts of CCl_4 laterally dispersed, dissolved in the aqueous phase, sorbed to the porous media, and as vapor compared with the layered geologic models. The pedotransfer function heterogeneous geologic realizations had generally higher intrinsic permeabilities, which resulted in nearly all of the disposed CCl_4 migrating out of the domain prior to the initiation of SVE in 1993. These results are inconsistent with the field extractions of about 54,000 kg CCl_4 via SVE operations at the 216-Z-9. The SMS method heterogeneous geologic realizations yielded lower DNAPL vertical migrations, but higher gaseous CCl_4 migration compared with the layered geologic models, with the most significant difference being that no DNAPL crossed the water table in the SMS simulations. The results of this approach are non inconsistent with the actual 54,000 kg removed from the 216-Z-9 subsurface because more than this amount was predicted to be present at the start of the SVE campaign. All simulations showed preferentially vertical DNAPL migration, such that the center of mass remains centered beneath the disposal area.

The results and conclusions from these simulations of CCl_4 distribution through the vadose zone and into the groundwater, as reported in this paper and by Oostrom et

al. (2004; 2006; 2007), may provide useful information for assessing potential vadose zone remediation approaches. Estimates for the phase distribution of CCl_4 in the vadose zone and the type of continuing CCl_4 flux to the groundwater, along with a comparison to the site characterization data, can be used to establish appropriate targets for vadose zone remediation and assessment of appropriate technologies for these target volumes and the physical state of CCl_4 within these target volumes.

Simulations of SVE performance, while not necessarily required for the feasibility study, may be a useful component for design and implementation of an SVE system if this technology is selected as part of the continued remedial action for CCl_4 in the vadose zone. Of particular importance may be simulation of how the CCl_4 retained within the Cold Creek Units volatilizes, migrates in the vapor phase over time, and is impacted by SVE. Coupled vadose zone and groundwater simulations are also a potentially important component for implementation of remedies for the vadose zone and groundwater to assess the overall fate of CCl_4 and the impact of the CCl_4 flux from the vadose zone to the groundwater. For instance, if the primary flux of CCl_4 from the vadose zone to the groundwater is via vapor phase interaction at the water table, it may be important to quantify this flux relative to the attenuation capacity of the aquifer and the capacity and longevity of any groundwater remediation technologies.

ACKNOWLEDGEMENTS

Simulations reported in this paper were conducted on the MPP2 supercomputer at the Molecular Science Computing Facility (MSCF) in the William R. Wiley Environmental Molecular Sciences Laboratory (EMSL), a national scientific user facility sponsored by the U.S. Department of Energy's Office of Biological and Environmental Research and located at the Pacific Northwest National Laboratory (PNNL). These simulations were performed under a Computational Grand Challenge Application project, "Multifluid Flow and Multicomponent Reactive Transport in Heterogeneous Subsurface Systems". The residual DNAPL saturations were obtained in the Subsurface Flow and Transport Experimental Laboratory at the EMSL. Development of the experimental procedures to determine residual DNAPL

saturations was funded by the Remediation and Closure Science Project through the U.S. Department of Energy's Richland Operations Office. PNNL is operated by Battelle for the DOE.

REFERENCES

Brooks, R. H. and A. T. Corey. 1964. "Hydraulic Properties of Porous Media." Hydrol. Pap. 3, Civil Engineering Department, Colorado State University, Fort Collins, Colorado.

Burdine, N.T. 1953. Relative permeability calculations from pore-size distribution Data. Petr. Trans., Am. Inst. Mining Metall. Eng. 198:71-77.

Cardwell, W. T., and R. L. Parsons. 1945. Average Permeabilities of Heterogeneous Oil Sands. Trans. Am. Inst. Mining Met. Pet. Eng. 160:34-42.

DOE. 2002. Standardized Stratigraphic Nomenclature for Post-Ringold Formation Sediments Within the Central Pasco Basin. DOE/RL-2002-39. U.S. Department of Energy, Richland, WA.

Deutsch C. V. and A. G. Journel. 1998. GSLIB – Geostatistical Software Library and User's Guide. Oxford University Press Inc., New York.

Ellerd, M. G., J. W. Massmann, D.P. Schwaegler, and V.J. Rohay. 1999. Enhancements for passive vapor extraction: The Hanford study. Ground Water 37 (3), 427-437.

Falta R.W., K. Pruess, I. Javandel, and P.A. Witherspoon. 1992. Numerical modeling of steam injection for the removal of nonaqueous phase liquid from the subsurface. 1. Numerical formulation. Water Resour. Res. 21:587-596.

Gropp, W., E. Lusk, A., and A. Skjellum. 1999. Using MPI: Portable Parallel Programming with the Message Passing Interface, 2nd edition. MIT Press, Cambridge, MA.

Huyakorn, P. S., S. Panday, and Y. S. Wu. 1994. A 3-Dimensional Multiphase Flow Model for Assessing NAPL Contamination in Porous and Fractured Media: 1. Formulation. Journal of Contaminant Hydrology 16(2):109-130.

Johnson, D. N., J. A. Pedit, and C. T. Miller. 2004. Efficient, near-complete removal of DNAPL from three-dimensional, heterogeneous porous media using a novel combination of treatment technologies. Environ. Sci. Technol. 38:5149–5156.

Khaleel R. and E. J. Freeman. 1995. Variability and Scaling of Hydraulic Properties for 200 Area Soils, Hanford Site. WHC-EP-0883, Westinghouse Hanford Company, Richland, Washington.

Khaleel R., T. E. Jones, A. J. Knepp, F. M. Mann, D. A. Myers, P. M. Rogers, R. J. Serne, and M. I. Wood. 2001. Modeling Data Package for S-SX Field Investigation Report (FIR). RPP-6296 Rev. 0, CH2MHILL Hanford Group, Inc., Richland, WA.

Klinkenberg L.J. 1941. The Permeability of Porous Media to Liquids and Gases. *In* Drilling and Production Practice p. 200-213, American Petroleum Institute, New York.

Last, G. V., Rohay, V. J., 1993. Refined Conceptual Model for the Volatile Organic Compounds-Arid Integrated Demonstration and 200 West Area Carbon Tetrachloride Expedited Response Action. PNL-8597/UC-630, Pacific Northwest Laboratory, Richland, Washington.

Lenhard, R.J., J.C. Parker, and S. Mishra. 1989. On the correspondence between Brooks-Corey and van Genuchten models. J. of Irrigation and Drainage Engineering 115:744-751.

Li D., B. Beckner, and A. Kumar. 2001. A new efficient averaging technique for scaleup of multimillion-cell geologic models. SPE Reservoir Evaluation and Engineering, 8:297-307.

Malik M. A. and L. W. Lake. 1997. A practical approach to scaling-up permeability and relative permeabilities in heterogeneous permeable media. Paper SPE 38310, presented at the 1997 SPE Western Regional Meeting, Long Beach, California, 25-27 June.

Massmann, J. W., 1989. Applying groundwater flow models in vapor extraction system design. Journal of Environmental Engineering 115(1), 129-149.

Miller, E. E., and R. D. Miller. 1956. Physical Theory for Capillary Flow Phenomena. J. Appl. Phys. 27:324-332.

Mualem, Y. 1976. A new model for predicting the hydraulic conductivity of unsaturated porous media. Water Resour. Res. 12:513-522.

Oostrom M., M. L. Rockhold, P. D. Thorne, G. V. Last, and M. J. Truex. 2004. Three-Dimensional Modeling of DNAPL in the Subsurface of the 216-Z-9 Trench at the Hanford Site. PNNL-14895, Pacific Northwest National Laboratory.

Oostrom, M., M. D. White, R. J. Lenhard, P. J. van Geel and T. W. Wietsma. 2005. A comparison of models describing residual NAPL formation in the vadose zone. Vadose Zone Journal. 4:163-174.

Oostrom, M., M. L. Rockhold, P. D. Thorne, G. V. Last, and M. J. Truex. 2006. Carbon Tetrachloride Flow and Transport in the Subsurface of 216-Z-9 Trench at the Hanford Site: Heterogeneous Model Development and Soil Vapor Extraction Modeling. PNNL-15914, Pacific Northwest National Laboratory.

Oostrom, M., M. L. Rockhold, P. D. Thorne, G. V. Last, M. J. Truex, and V.J. Rohay. 2007. Carbon tetrachloride flow and transport in the subsurface of the 216-Z-9 trench at the Hanford Site. Vadose Zone Journal. In press.

Piepho, M. G. 1996. Numerical Analysis of Carbon Tetrachloride Movement in the Saturated and Unsaturated Zones in the 200 West Area, Hanford Site. Bechtel Hanford, Inc., BHI-00459, Richland, Washington.

Renard, Ph., and G. de Marsily. 1997. Calculating equivalent permeability: A Review. Adv. Water Resour. 20:253-278.

Rockhold, M. L. 1999. Parameterizing Flow and Transport Models for Field-Scale Applications in Heterogeneous, Unsaturated Soils. In Assessment of Non-Point Source Pollution in the Vadose Zone, D.L. Corwin, K. Loague, and T. R. Ellsworth (eds.), American Geophysical Union, Geophysical Monograph 108, pp. 243-260.

Rockhold M. L., M. J. Fayer, and P. R. Heller. 1993. Physical and Hydraulic Properties of Sediments and Engineered Materials Associated with Grouted Double-Shell Tank Waste Disposal at Hanford. PNL-8813, Pacific Northwest Laboratory, Richland, Washington.

Rosing, M., 2000. DL Tutorial and Manual, Version 1.0. Peak Five, Fort Collins, Colorado, USA. Available at http://www.peakfive.com.

Rosing, M., Yabusaki, S., 1999. A programmable preprocessor for parallelizing Fortran-90. In Proceedings of the IEEE/ACM SC99 Conference, November 13 - 18, 1999, Portland, Oregon, USA

van Genuchten, M. 1980. A closed-form equation for rredicting the hydraulic conductivity of unsaturated soils. Soil Sci. Am. J. 44:892-898.

Ward, A. L., M. D. White, E. J. Freeman, and Z. F. Zhang. 2005. STOMP: Subsurface Transport Over Mulitple Phases, Version 1.0, Addendum: Sparse Vegetation Evapotranspiration Model for the Water-Air-Energy Operational Mode. PNNL-15465, Pacific Northwest National Laboratory, Richland, Washington.

White, M. D., Oostrom, M., 2000. STOMP Subsurface Transport Over Multiple Phases, Version 2.0, Theory Guide. PNNL-12030, UC-2010, Pacific Northwest National Laboratory, Richland, Washington.

White, M. D., M. Oostrom, and R. J. Lenhard. 2004. A practical model for mobile, residual, and entrapped NAPL in water-wet porous media. Ground Water. 42(5):734-746.

White, M. D., B. P. McGrail. 2005. STOMP Subsurface Transport Over Multiple Phases, Version 1.0, Addendum: ECKEChem Equilibrium-Conservation-Kinetic Equation Chemistry and Reactive Transport. PNNL-15482, Pacific Northwest National Laboratory, Richland, Washington.

White, M. D., and M. Oostrom. 2006. STOMP Subsurface Transport Over Multiple Phases, Version 4.0, User's Guide. PNNL-15782, Pacific Northwest National Laboratory, Richland, WA.

Table 1. Laboratory-determined properties of the 216 Z-9 DNAPL mixture (after Oostrom et al., 2007).

Density (kg m^{-3})	1,426
Viscosity (Pa s)	1.11×10^{-3}
Vapor Pressure (Pa)	10,830
Surface Tension (dynes/cm)	25.1
Interfacial Tension (dynes/cm)	15.2
Aqueous Solubility (g/L)	0.75

Table 2. DNAPL and aqueous phase disposal rates and volumes for the 216-Z-9 disposal site. The infiltration area (footprint) of the site is 167.2 m^2.

	DNAPL		**Aqueous Phase**	
Period	*Rate (m^3/year/m^2)*	*Volume (m^3)*	*Rate (m^3/year/m^2)*	*Volume (m^3)*
7/1955 through 12/1955	0.062	5	3.04	255
1956	0.277	46	2.47	414
1957	0.277	46	2.95	494
1958	0.265	45	3.92	655
1959	0.283	47	3.07	513
1960	0.286	48	3.42	572
1961	0.379	63	4.23	707
1/1962 through 6/1962	0.178	15	1.98	165
Total		*315*		*3,770*

Table 3. Saturated hydraulic conductivity (K_s), porosity (n), and retention parameter values (Brooks-Corey air-entry pressure head h_d, pore geometry factor λ, and irreducible water saturation, s_{rl}) of hydrostratigraphic units.

Stratigraphic Units	K_s **(cm/s)**	n	h_d **(cm)**	λ	s_{rl}
Ringold A	5.73E-3	0.0770	71.3	0.52	0.1299
Lower Mud	1.16E-8	0.0770	71.3	0.52	0.1299
Ringold E	5.73E-3	0.0770	71.3	0.52	0.1299
Upper Ringold	5.73E-3	0.0770	71.3	0.52	0.1299
Cold Creek Unit Carbonate	6.72E-3	0.3203	36.3	0.61	0.2451
Cold Creek Unit Silt	1.48E-4	0.4238	120.0	0.79	0.0967
Lower Sand	1.87E-2	0.3359	4.7	0.78	0.0747
Lower Gravel	3.00E-2	0.2720	23.0	0.75	0.1471
Hanford 2	5.85E-3	0.3653	14.1	0.95	0.0846
Hanford 1	5.00E-2	0.1660	7.7	0.54	0.1386
Hanford 1A	5.98E-4	0.4478	58.1	0.71	0.1740
Backfill	1.5E-2	0.2620	22.0	0.36	0.3646

1
2

Table 4. Total DNAPL mass inventory and DNAPL mass in vadose zone at 1993 as a percentage of total inventory for the layered and similar media grid refinement simulations

Simulation	Total DNAPL mass inventory (kg)	DNAPL mass (kg) in vadosezone at 1993	DNAPL Mass (kg) in vadose zone at 1993 as a percentage of inventory
Layered			
78K	4.50E5	1.93E5	43
310K	4.50E5	2.16E5	48
635K	4.50E5	2.31E5	51
1075K	4.50E5	2.32E5	51
Similar Media Scaling			
78K	4.50E5	1.08E5	24
310K	4.50E5	1.19E5	26
635K	4.50E5	1.33E5	30
1075K	4.50E5	1.34E5	30

Table 5. Total DNAPL mass inventory, time for DNAPL to reach the water table, and DNAPL mass transported across the water table at 1993 for the layered and similar media scaling grid refinement simulations

Simulation	Total DNAPL mass inventory (kg)	Time (yr) for DNAPL to reach water table	DNAPL Mass (kg) moved across water table at 1993
Layered			
78K	4.50E5	9.0	26,744
310K	4.50E5	8.4	32,621
635K	4.50E5	7.9	36,016
1075K	4.50E5	7.9	36,974
Similar Media Scaling			
78K	4.50E5	10.2	5,419
310K	4.50E5	12.7	1,218
635K	4.50E5	-	-
1075K	4.50E5	-	-

Table 6. Mean horizontal hydraulic conductivity values for layered model and Realization 1 for the heterogeneous models based on the PDF and similar media scaling methods.

Hydrostratigraphic unit	Layered model	Heterogeneous model PDF method	Heterogeneous model similar media scaling method
Basalt	1.16E-08	1.16E-07	1.16E-08
Ringold A	5.73E-03	9.43E-02	3.78E-02
Lower Mud	1.16E-08	1.14E-01	1.22E-07
Ringold E	5.73E-03	8.50E-02	8.57E-03
Upper Ringold	5.73E-03	5.42E-02	1.85E-03
Cold Creek carbonate	6.72E-03	6.72E-02	6.72E-03
Cold Creek silt	1.48E-04	1.19E-02	1.05E-04
Lower Sand	1.87E-02	5.19E-02	2.01E-02
Lower Gravel	3.00E-02	5.30E-02	2.06E-02
H2	5.85E-03	8.02E-02	6.71E-03
H1	5.00E-02	2.32E-01	9.77E-02
H1a	5.98E-04	3.37E-02	2.11E-03

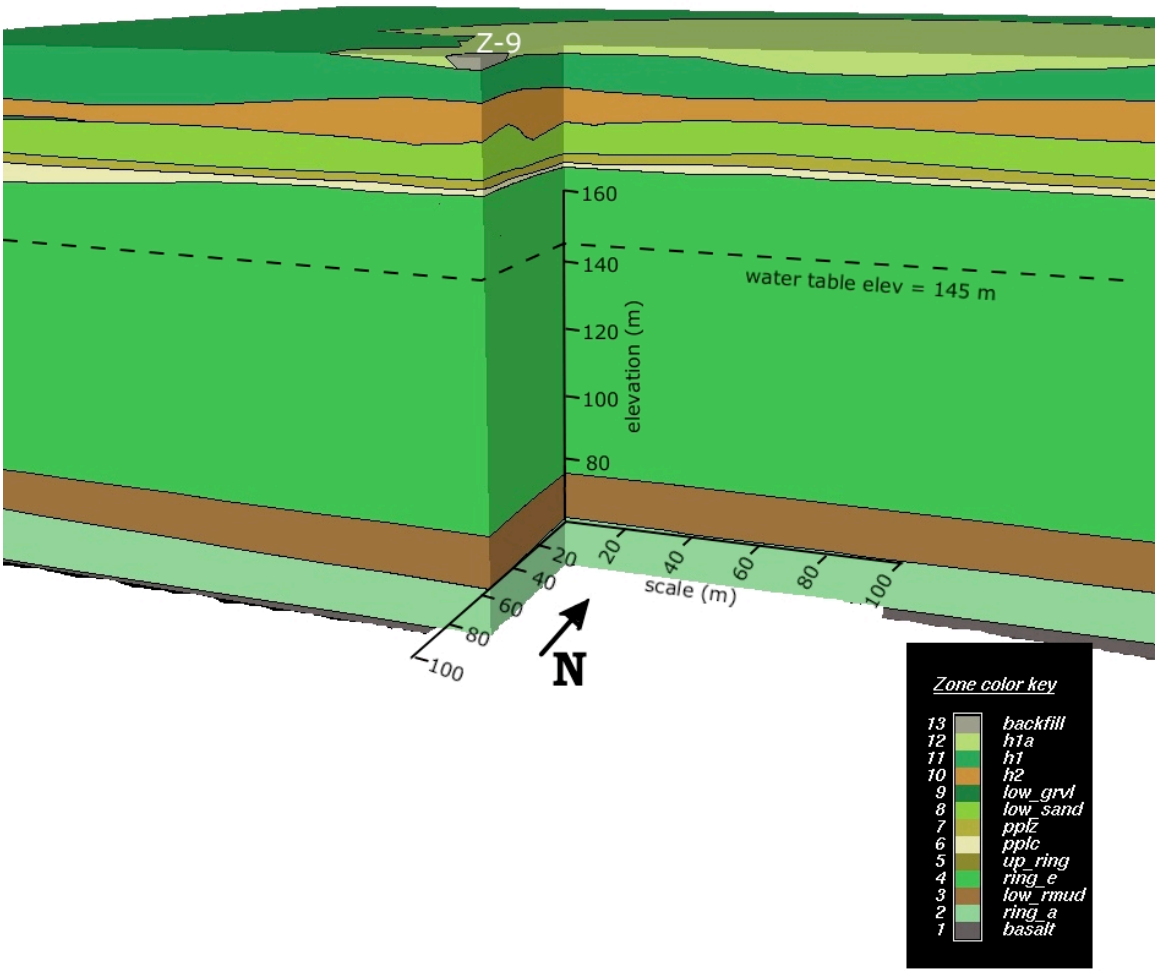

Figure 1. Three-dimensional geologic domain with a cut-out below the 216-Z-9 trench. The stratigraphic units in the legend denote Backfill, Hanford 1a (h1a), Hanford 1 (h1), Hanford 2 (h2), Lower Gravel (low_grvl), Lower Sand (low_sand), Cold Creek Unit Silt (pplz), Cold Creek Unit Carbonate (pplc), Upper Ringold (up_ring), Ringold E (ring_e), Ringold Lower Mud (low_rmud), Ringold A (ring_a), and Basalt.

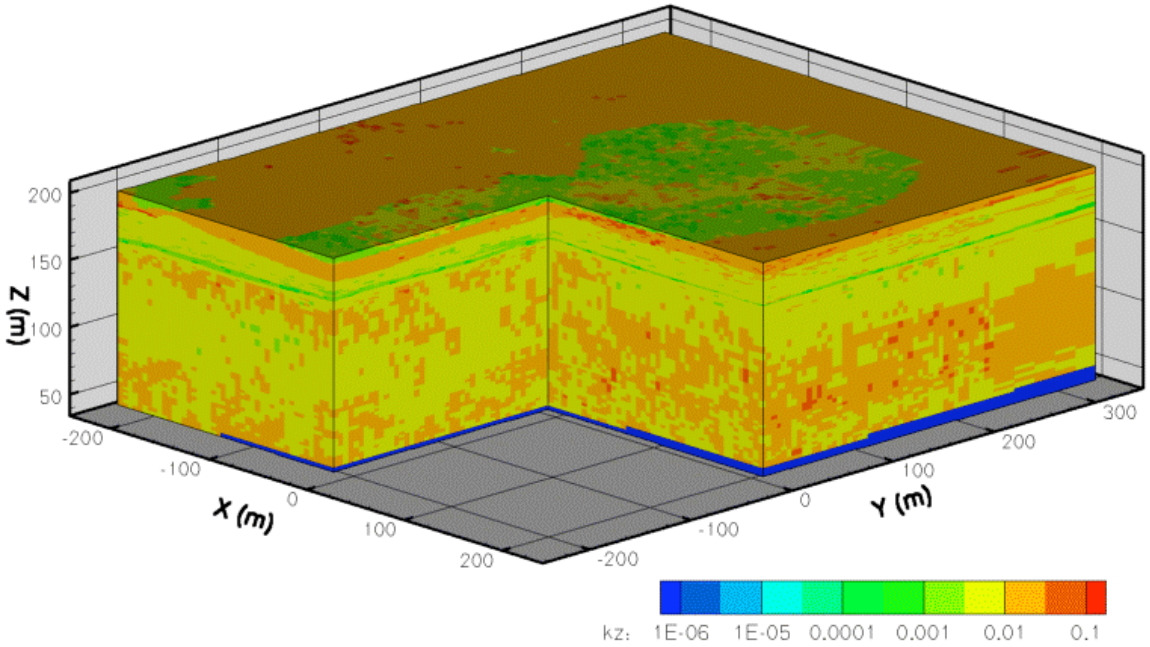

Figure 2a. Vertical saturated hydraulic conductivity (cm/s) on the computational domain from the pedotransfer function method.

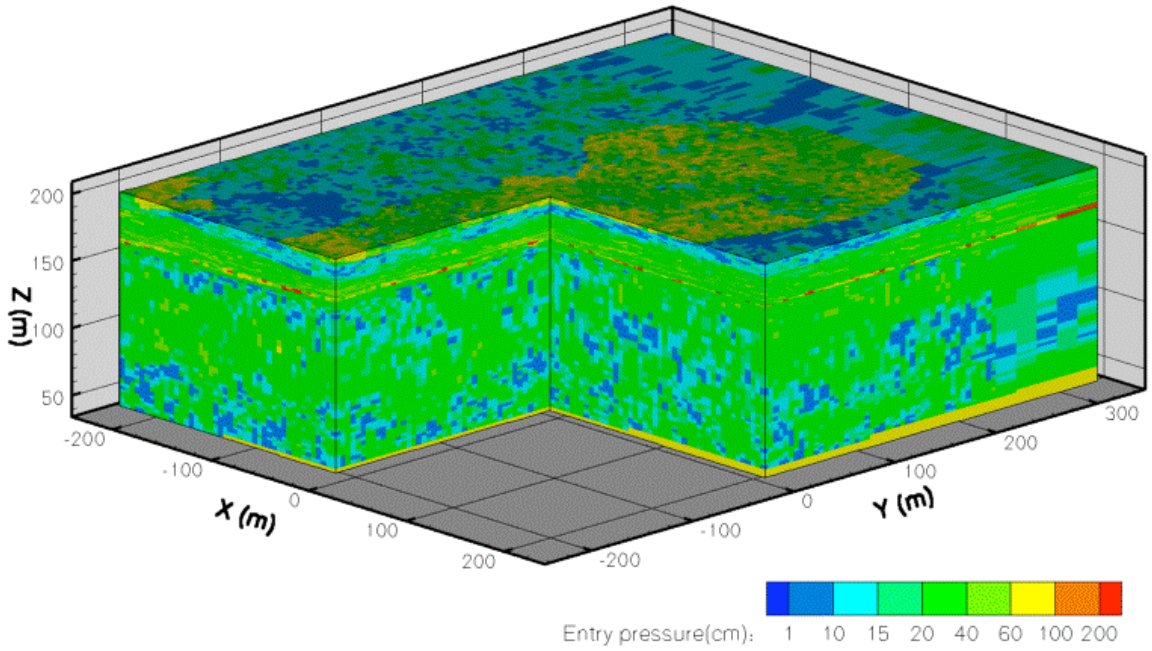

Figure 2b. Brooks-Corey entry pressure head (cm) on the computational domain from the pedotransfer function method.

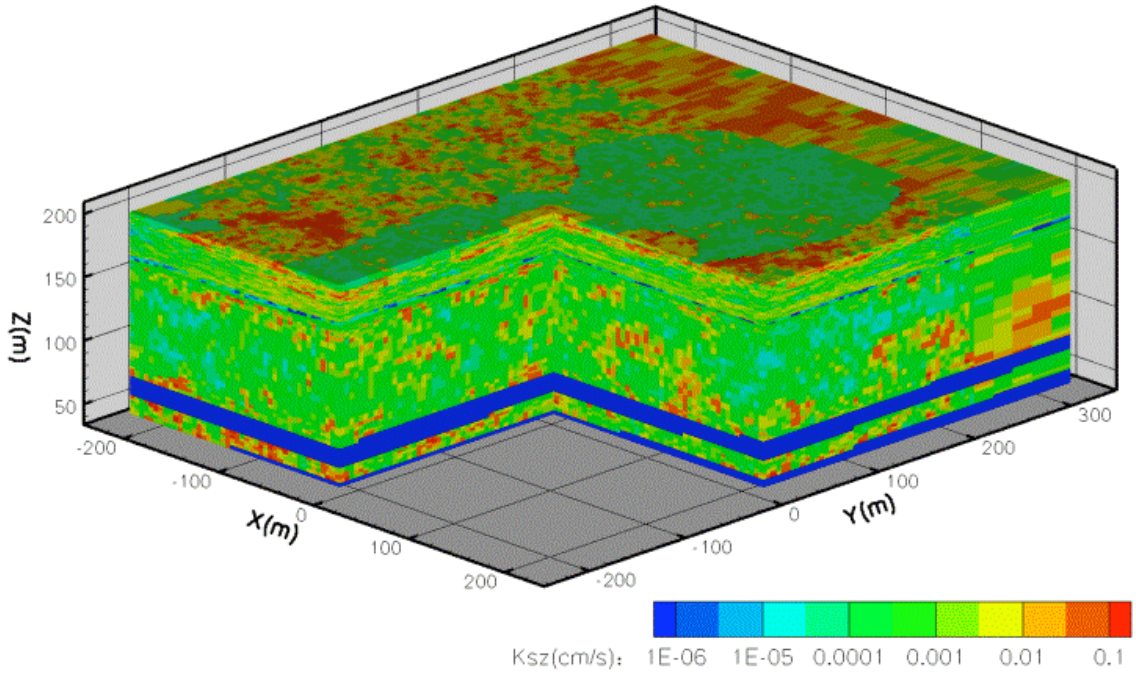

Figure 3a. Vertical saturated hydraulic conductivity (cm/s) on the computational domain from the similar media scaling method.

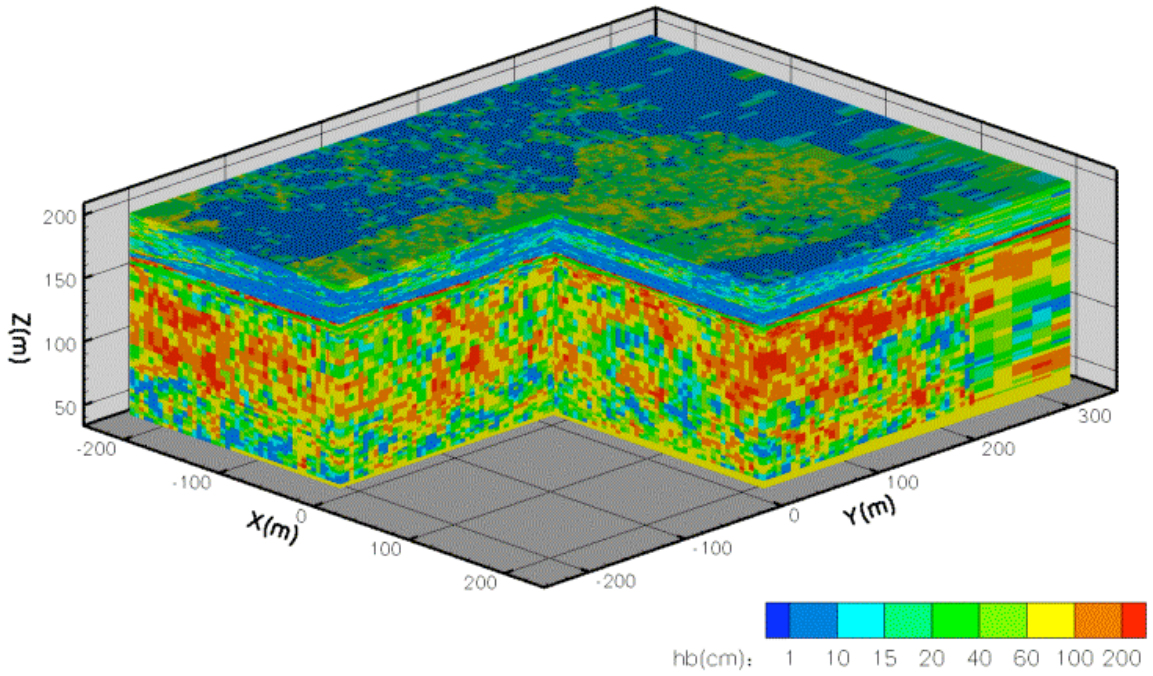

Figure 3b. Brooks-Corey entry pressure head (cm) on the computational domain from the similar media scaling method.

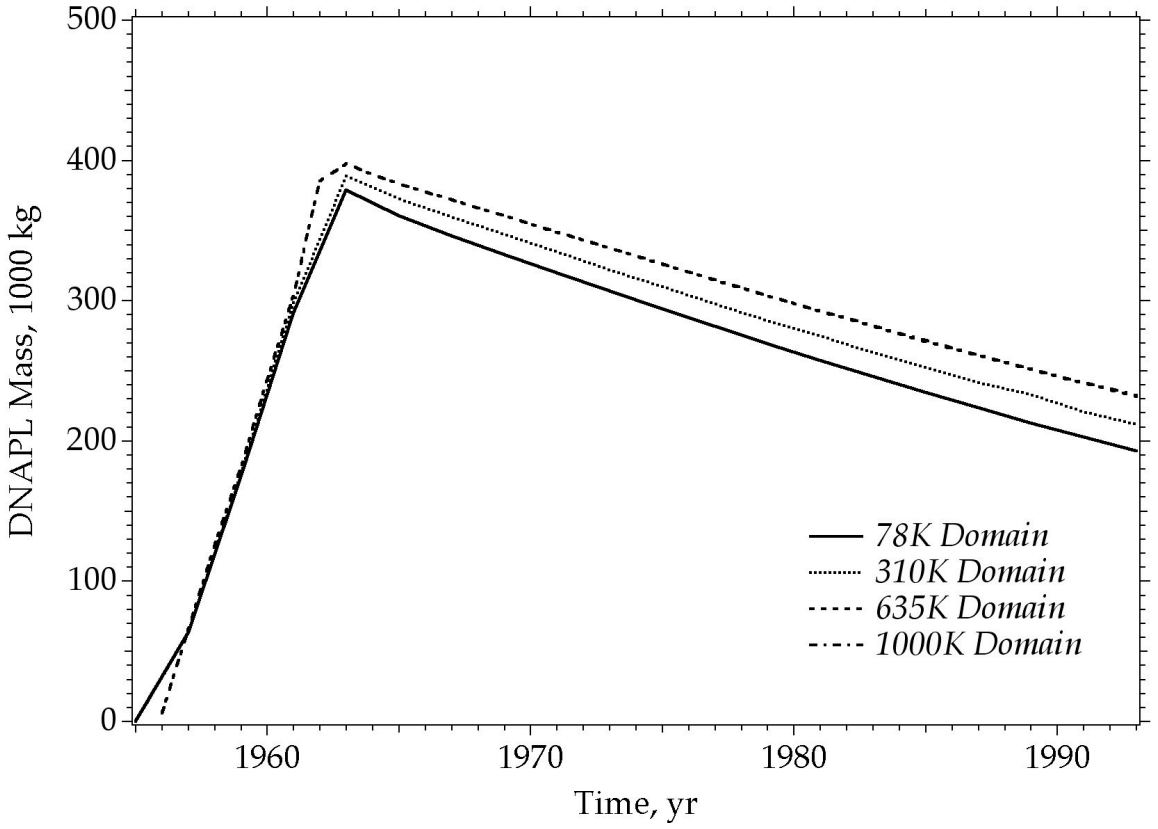

Figure 4. DNAPL Mass (kg) in the computational domain for the 78K, 310K, 635K, and 1075K layered simulations between 1955 and 1993.

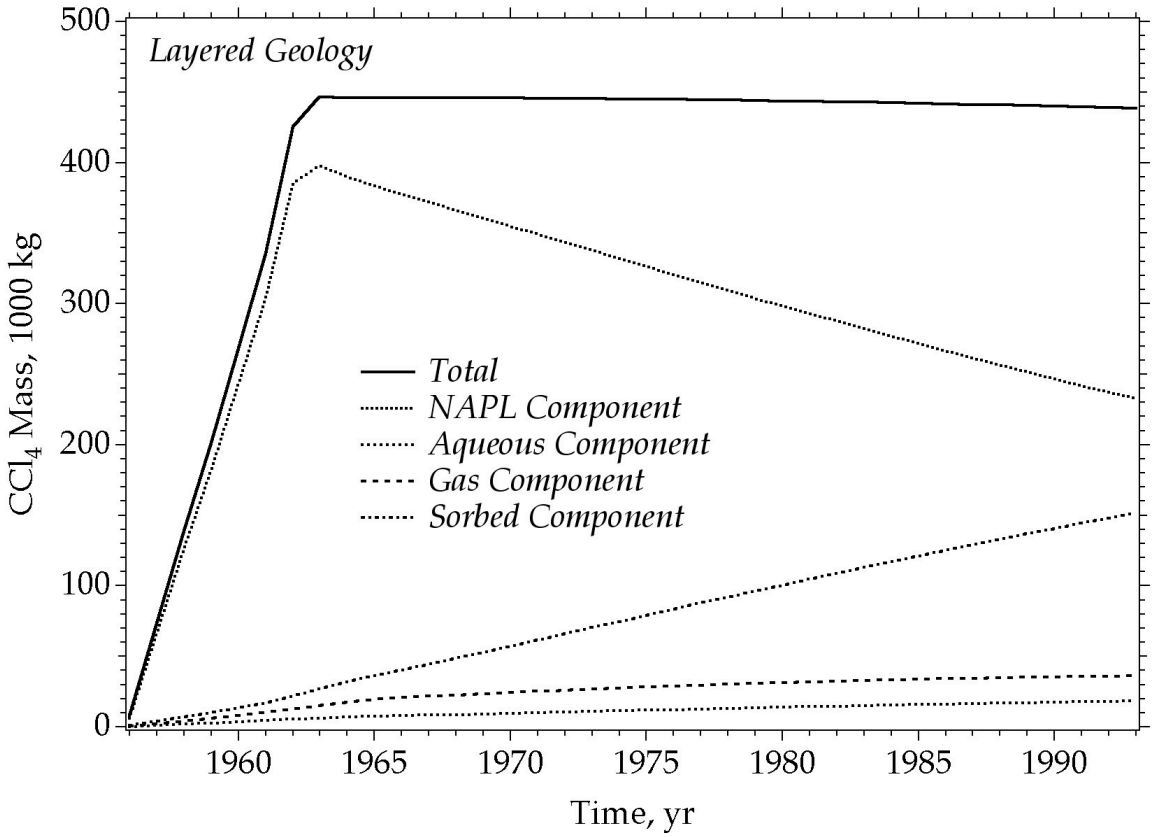

Figure 5a. CCl_4 phase distribution versus time for the layered geology (1075K grid).

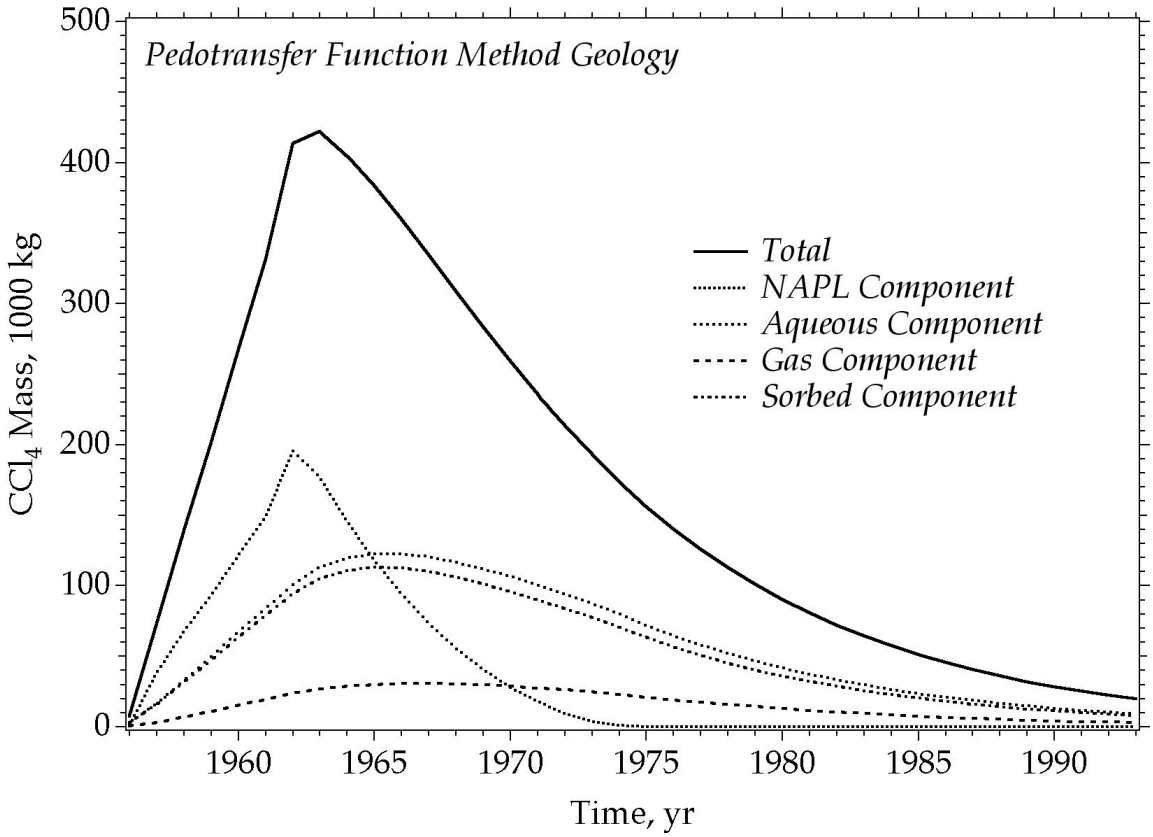

Figure 5b. CCl_4 phase distribution versus time for the pedotransfer function method (1075K grid).

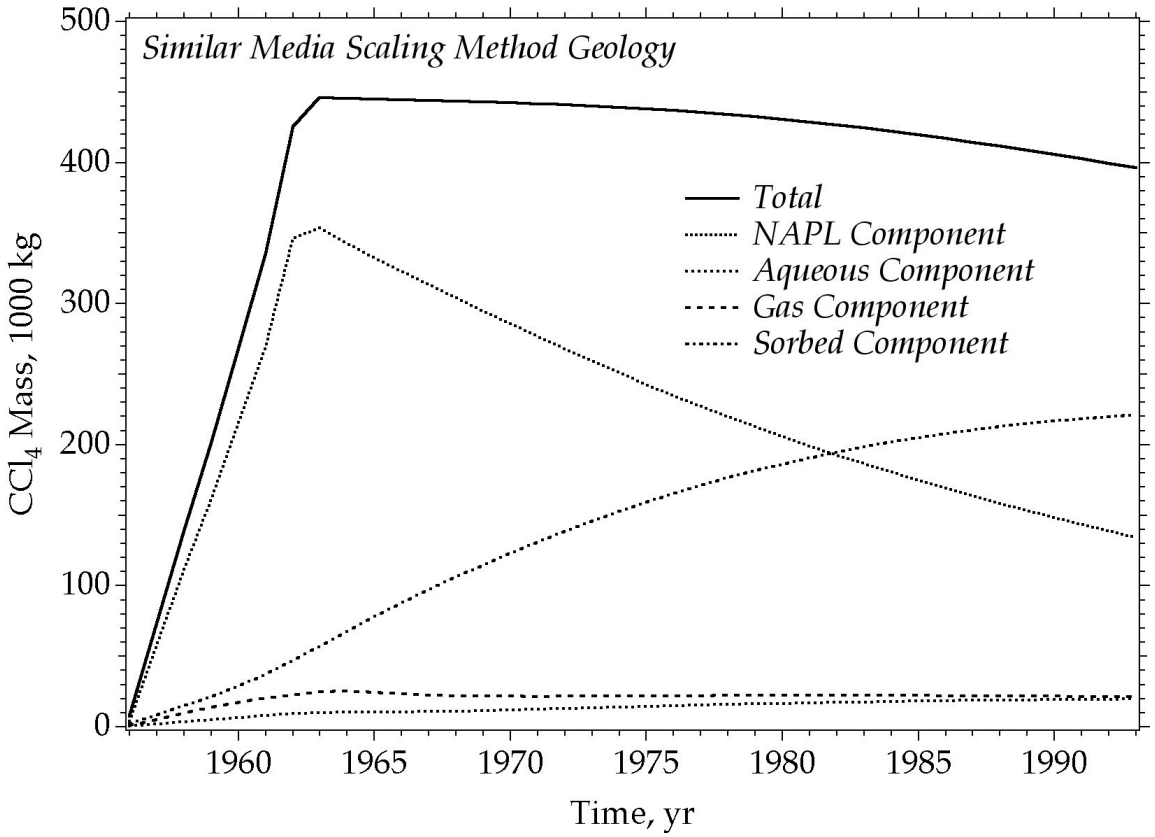

Figure 5c. CCl_4 phase distribution versus time for the similar media scaling method (1075K grid).

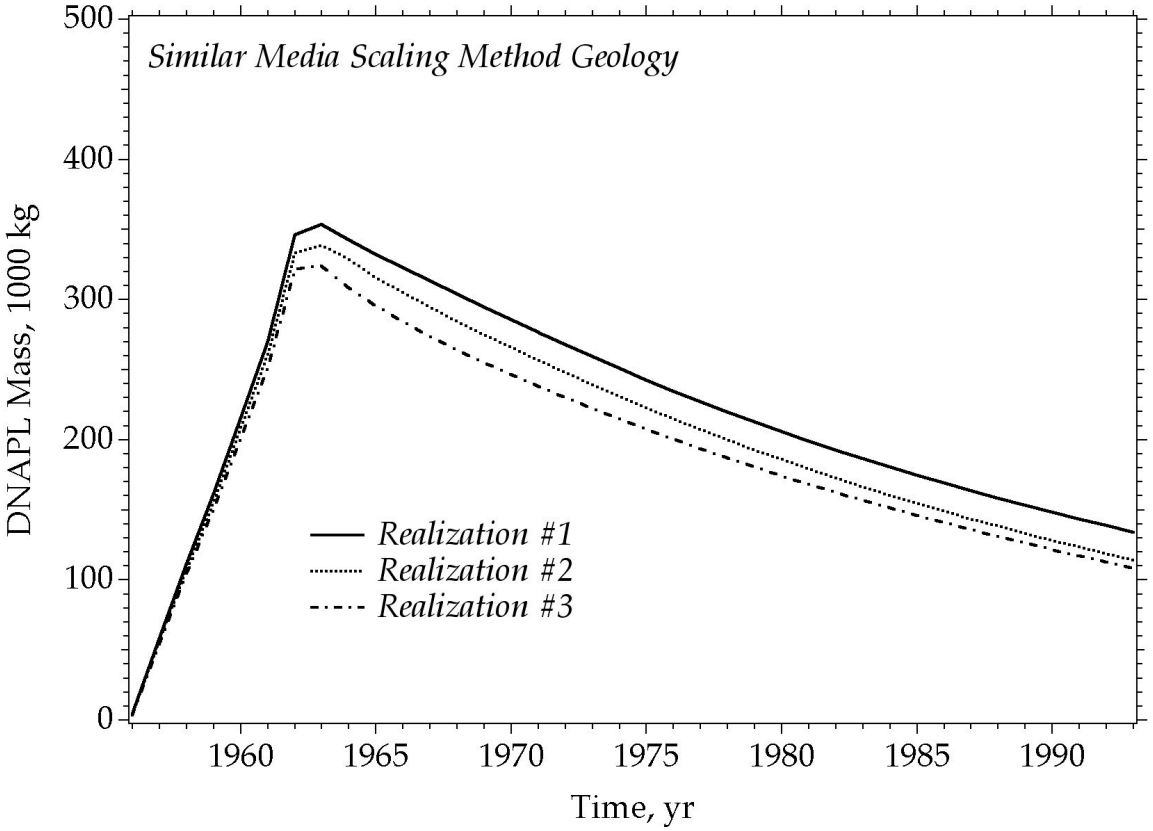

Figure 6. Comparison of DNAPL mass in the computational domain as a function of time for the three realizations based on the similar media scaling method.

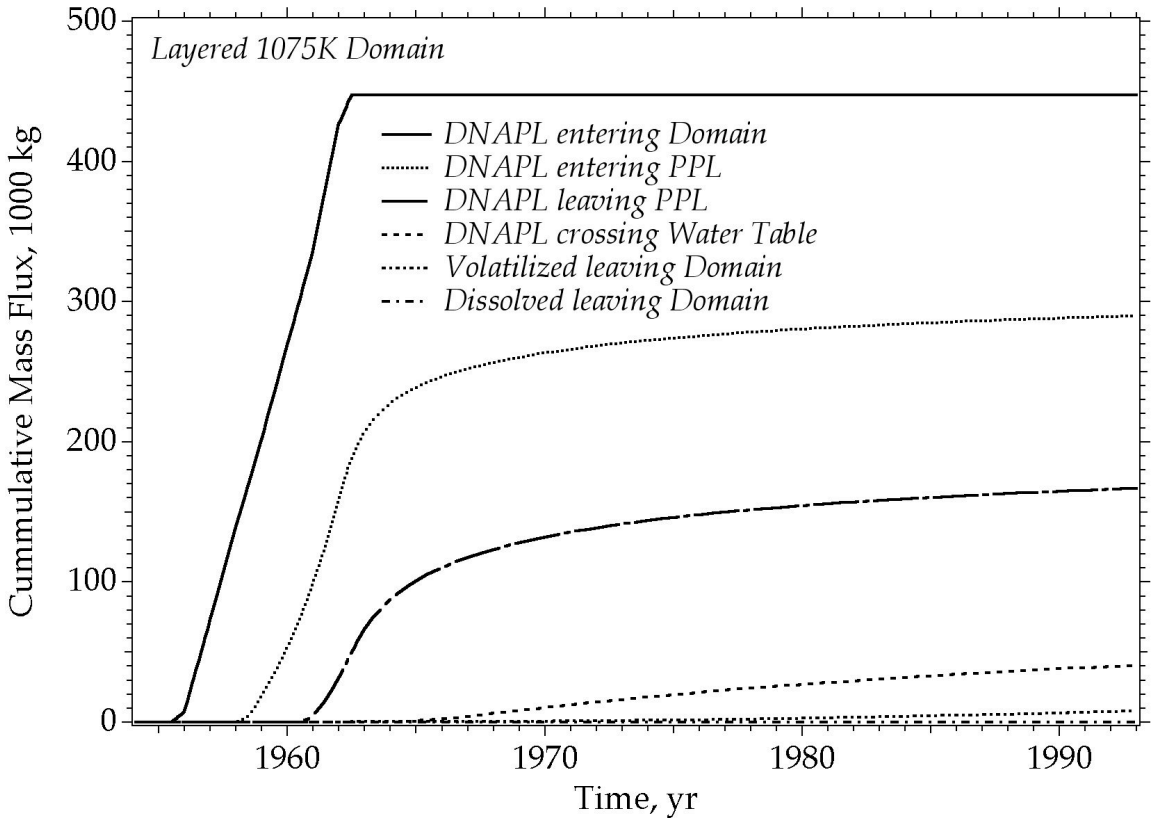

Figure 7a. Cumulative DNAPL and dissolved mass fluxes for the layered 1075K node simulation. The abbreviation PPL denotes the Cold Creek Units.

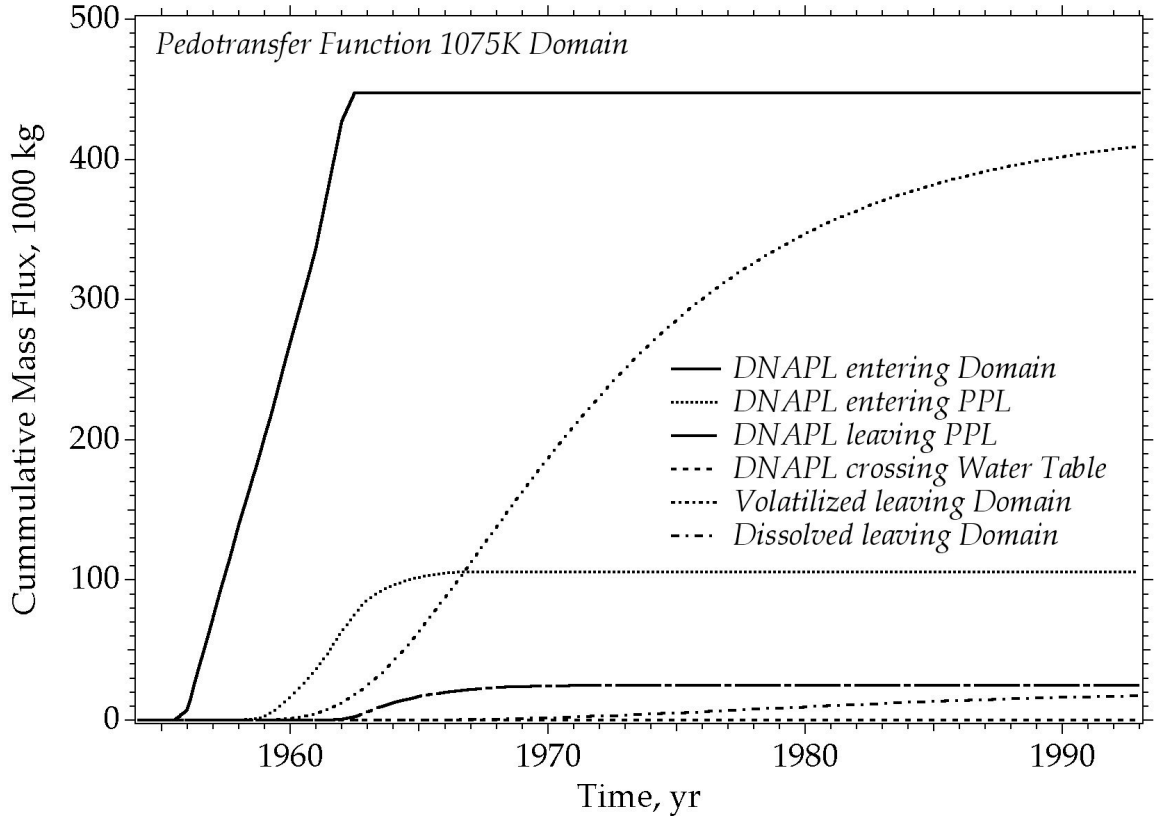

Figure 7b. Cumulative DNAPL and dissolved mass fluxes for realization 1, heterogeneous 1075K node simulation based on the pedotransfer function method. The abbreviation PPL denotes the Cold Creek Units.

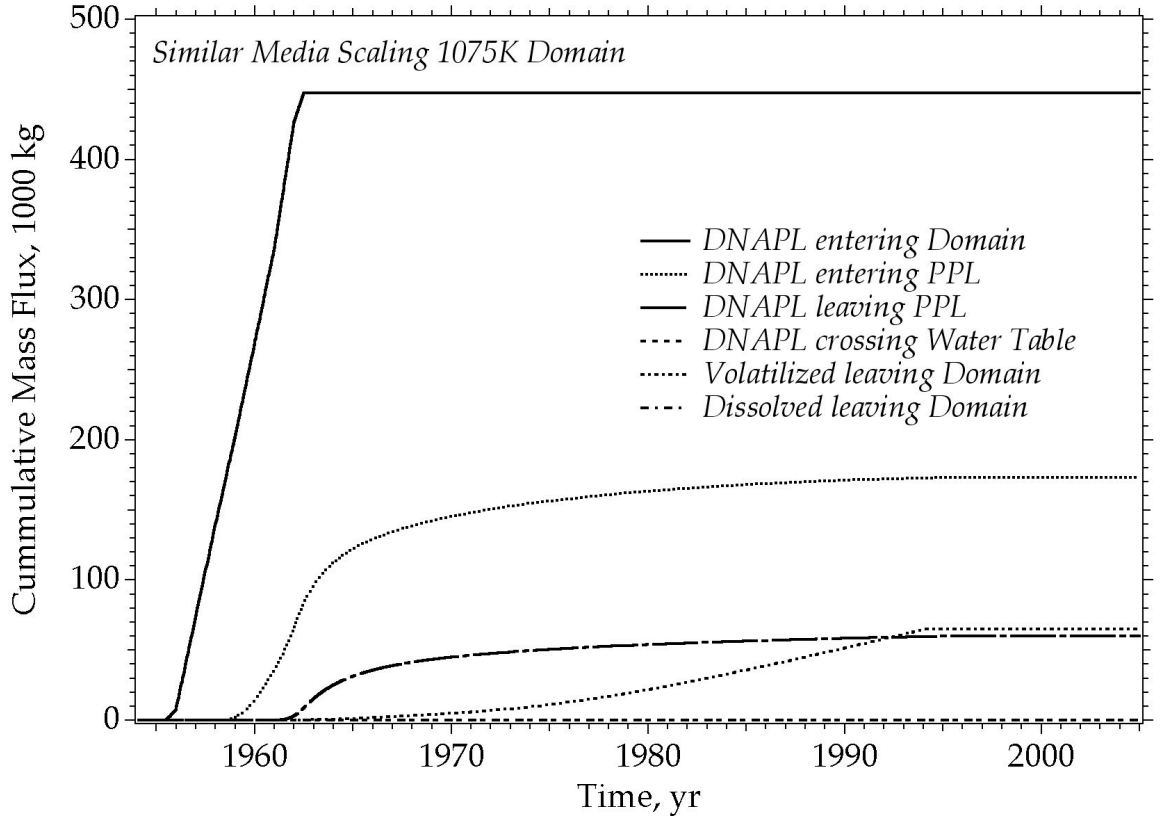

Figure 7c. Cumulative DNAPL and dissolved mass fluxes for Realization 1, heterogeneous 1075K node simulation based on the similar media scaling method. The abbreviation PPL denotes the Cold Creek Units.

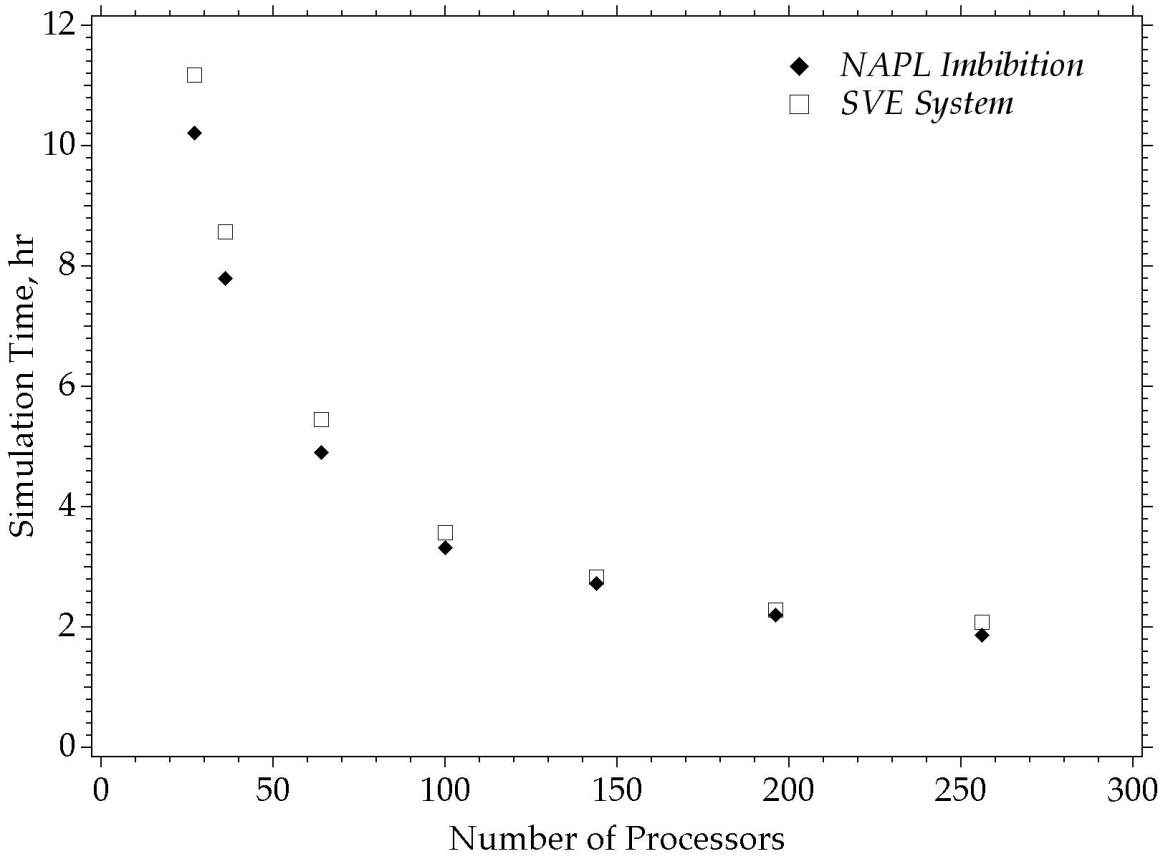

Figure 8. Scaling performance: Execution time versus number of processors for fixed number of unknowns (3,225K).